HYPOTHESIS

OPEN ACCESS

Effect of ZnO (Zinc Oxide) and CeO$_2$ (Cerium IV Dioxide) Nanoparticles on 16HBE14o Bronchial Epithelial Cells Pro-inflammatory Cytokine Secretory Phenotype

Abisoye Muyideen Olaifa*

BSc Hons Immunology & Pharmacology (Aberdeen, 2015); Postgraduate Genetics (UCLan, 2019) DofE Gold (2012), UK.

Abstract

Background: Airway Epithelial Cells (AECs) are the first line of defence against inhaled microbes and pollutants from the environment including nanoparticles. Unresolved AEC injury is proposed to contribute to Th2 inflammation and asthma pathogenesis. **Aim:** To determine the cytotoxic effects of and the pro inflammatory secretory phenotype of 16HBE14o bronchial epithelial cells dosed with ZnO and CeO$_2$ nanoparticles. **Methods:** 16HBE14o bronchial epithelial cells were cultured and their identity confirmed using immunocytochemistry. Cultured confluent monolayers of 16HBE14o were dosed with increasing concentrations of ZnO and CeO$_2$ nanoparticles. An acid phosphatase assay was carried out to determine the cytotoxic effect of the nanoparticles on the cell line. Further, ELISAs were used to determine the concentration of IL-8 and IL-33 in supernatants from control and nanoparticle treated 16HBE14o. Finally apoptosis assays and measurements of ROS were carried out. **Results:** High ZnO nanoparticle concentrations (50 µg/ml and 100 µg/ml) had cytotoxic effects on 16HBE14o cells. Low ZnO nanoparticle Concentrations (2.5 µg/ml to 25 µg/ml) induced the secretion of IL-8 but not IL-33 by 16HBE14o bronchial epithelial cells. Low concentrations of both ZnO and CeO$_2$ nanoparticles induce ROS production in 16HBE14o cells. Cerium dioxide had no significant effect in any of the other assays. **Conclusion:** ZnO nanoparticles are cytotoxic on 16HBE14o cells via necrosis. ZnO nanoparticles cause IL-8 production in 16HBE14o cells.

Keywords: Nanoparticle, Zinc Oxide (ZnO), Cerium dioxide (CeO$_2$), Th2 inflammation, 16HBE14o, Airway Bronchial Epithelial Cells, IL-8, IL-33

Introduction

Much is said and implemented regarding the damaging effects of the industrial revolution and climate change on our planet. From the legally binding Paris agreement instituted at the United Nations Conference of Parties, COP 21 and signed on the 22nd of April 2016 to the annual Earth shot prize which aims to reverse global warming by financially incentivising breakthrough innovation in five areas namely: the restoration and protection of nature, air cleanliness, ocean revival, waste-free living and climate action. More people would take these climate discussions more seriously if, rather than entirely focusing on the effects of climate change on planet earth, we focused on what effect, if any, climate change driven by the human activities of the industrial revolution has on human health including air pollution, increased atmospheric concentrations of allergens and pollens, decreased lung function, preterm birth survival, antenatal, neonatal, congenital and adult development of respiratory diseases like asthma. This laboratory research project will shed some light [1,2].

Asthma is a chronic inflammatory disorder of the airways. It is one of the most common chronic diseases in developed nations. Approximately 10% of the worldwide population suffer from asthma. Asthma management and treatment is estimated to cost the UK National Health Service roughly £750 million a year. It is also estimated the cost the UK economy about £700,000 million through lost working days. Even with the availability of effective medication, there is increased frequency and severity of asthma

in developed nations. This trend is alleged to be due to a lack of depth and complete understanding of the pathogenesis of the disease, hence the suitability and appropriateness of this project. It aims to clarify the potential cytotoxic effect and pro inflammatory secretory phenotype induced by nanoparticles on airway epithelial cells.

The widely accepted philosophy around the pathogenesis of early onset atopic asthma is that it is allergy driven in genetically at risk individuals. The present understanding of the sequence of events is that exposure to allergens are processed by dendritic cells in the airway epithelium and presented to naïve CD^{4+} T cells to promote differentiation to Th^{-2} cells and stimulation of IgE class switching in B cells. This leads to Th2 inflammation and the production of IgE antibodies specific for the allergic antigen - followed by recruitment of associated mast cells, eosinophils, neutrophils, monocytes, basophils and additional CD^{4+} Th^{-2} cells to the conducting airway [3]. This view point has dominated understanding of asthma pathogenesis for a very long time and has informed the way in which therapy is designed and developed. This is despite the fact that the anti-inflammatory treatments developed fail to have any effect on the natural course of asthma and in a minority of patients with asthma can have a limited effect on the fully developed chronic disease. This is also despite the fact that late onset intrinsic asthma has an identical pathological phenotype without the obvious initiating allergic stimuli. This paradox casts a shadow of doubt on the soundness of understanding of asthma pathogenesis and suggests that other factors might be the initiating event

triggering Th2 airway inflammation [4].

Holgate et al., 2011 have suggested that rather than environmental allergens being the initiating factor, asthma is fundamentally initiated by damage to Airway Epithelial Cells (AECs). They suggest that the clinical pathological manifestations and starting point of asthma is the disruption of the barrier properties of the AECs. When the epithelial barrier is compromised, this renders the airway more susceptible to viral infection, environmental allergies and pollutants such as nanoparticles [4]. The latter are the focus of this project (FIGURE 1).

The production of cytokines by the AEC is thought to be crucial to the recruitment of infiltrating pro inflammatory cells to the airway following injury [5-7].

Further damage to the tight junctions, gap junctions, intermediate junctions and desmosomes that maintain the structural integrity of the epithelium provides the conditions necessary for the progression of acute inflammation to chronic inflammation leading to the phenomenon of airway remodelling. The bronchoconstriction that results leads to physical disruption of the epithelium. This physical disruption provides additional stimulus for more severe airway remodelling [8]. There is ample in vivo and in vitro evidence that epithelial barrier properties are damaged in asthma, together with reduced antioxidant activity and impaired innate immunity [9-12].

Further to epithelia barrier property damage being the initiating factor for airway remodelling, the relationship between the structural changes that result and the wound healing response which is usually incomplete have led to the description of the concept of EMTU (Epithelia Mesenchymal Trophic Unit) as being central to asthma pathogenesis.

The EMTU (FIGURE 2) can be defined as the anatomical and functional interaction between the epithelium, attenuated fibroblast sheath, neural tissue, smooth muscle and proteins of the extracellular matrix present underneath the basement membrane during foetal lung development in the womb and during asthma pathogenesis. It is thought that the EMTU pathway remains active after birth and is reactivated in asthmatics [13,14]. The environment provided by an activated EMTU allows the progression and perpetuation of Th2 initiated chronic inflammation even without the presence of an external initiating stimulus. An activated EMTU thus potentially provide an explanation for the cause of late onset intrinsic asthma induced in non-atopic individuals, as well as the full picture relating to the pathogenesis of early onset atopic asthma.

Linking asthma pathogenesis to an activated EMTU leads to a paradigm change. When the AECs are damaged by an environmental stimulus, they repair incompletely. This leads to the progression of acute inflammation
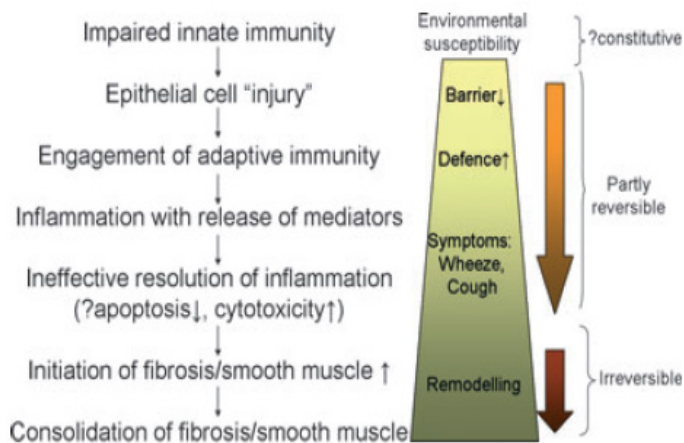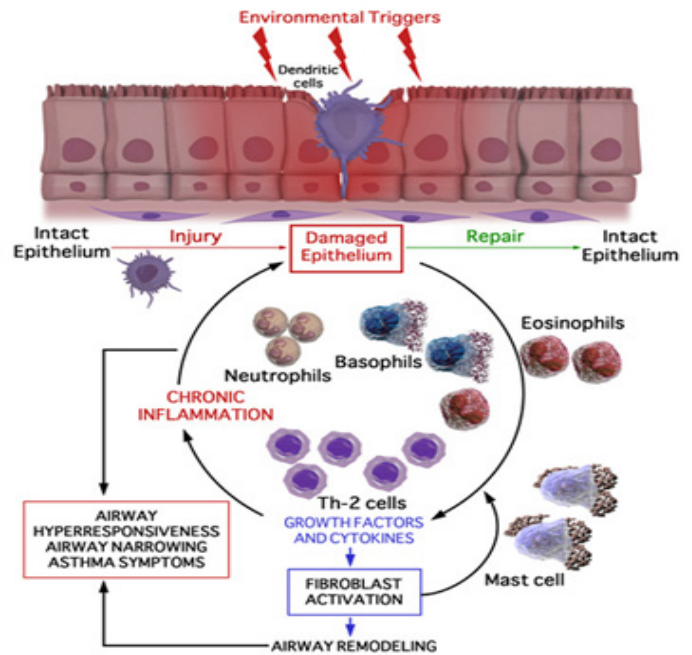
FIGURE 2. The relationship of epithelial-mesenchymal communication (epithelial-mesenchymal trophic unit) to persistent inflammation and airway wall remodelling. EGF, epidermal growth factor; TGF, tumour growth factor; CGRP, calcitonin gene related peptide; VEGF, vascular endothelial growth factor [4]

to chronic inflammation and a chronic wound scenario. This then leads to the secretion of several factors involved in AEC repair. These facilitate the structural changes that lead to the phenomenon of airway remodelling. These factors include the epidermal growth factor family and the fibroblast growth factor family. These have a role in the migration, proliferation and spreading of cells. IL-4 decreases cell movement. IFN-γ enhances cell movement. IL-13 through TGF-alpha and EGFR triggers proliferation and increases repair. IL-1β has a role in increasing cell movement and causing wound closure. PGE2, TGF-β, COX-1 and COX-2 have a role in wound closure. TGF-β also causes cell movement and reorganisation of the cell cytoskeleton [15,16].

Since recent experimental findings suggest that increased susceptibility to injury and altered repair rather than allergic stimulation are central to both the airway remodelling and mucous metaplastic responses in asthma, it follows that substances naturally present in the atmosphere including nanoparticles which could lead to increased AEC susceptibility to injury, cytokine production, altered incomplete repair and eventually the EMTU are potential culprits in asthma pathogenesis, especially since these substances are inhaled from birth [12,17].

IL-8 is a pro inflammatory cytokine and chemokine produced by bronchial epithelial cells and other cell types such as macrophages. Shibata et al, 1996 have shown that detached, deformed or injured AECs generate IL-8 which enhances the process of airway inflammation. IL-8 functions as a chemoattractant for the recruitment of eosinophils, neutrophils and T cells. It amplifies mediator release by these cells to enhance the inflammatory response [9]. The known stimuli for IL-8 production by AECs include IL-1, TNF-α, Para-Methoxyamphetamine, products of the gram negative bacteria, *Pseudomonas aeruginosa*, the globally distributed fungal pathogen, *Cryptococcus neoformans*, the Haemophilus influenza endotoxin, swine dust, viruses and Hog barn dust extract [15].

IL-33 is a recently described (2005) member of the IL-1 family of cytokines. It potently drives production of Th2 associated cytokines such as IL-4 and IL-13. IL-33 is required for the production of IL-13 by airway macrophages which drive mucous production and hypersensitivity [17]. It is expressed constitutively in AECs and produced by cells under

FIGURE 1. The pathophysiological processes implicated in the life course of asthma. Combinations of these give rise to the different asthma phenotypes and responses to interventions [4]

mechanical strain [19]. It also functions as an alarming, providing an endogenous danger signal when injury or tissue damage occurs. IL-33 is a ligand for the IL-33 receptor which is expressed on Th2 cells, eosinophils, basophils and mast cells. IL33 ultimately functions to increase innate Th2 immune response [20].

Nanoparticles are defined as particulate single substances with dimensions between 1 nm and 100 nm diameter. They can be naturally occurring in the atmosphere or are synthetic engineered nanoparticles. It is estimated that there are between 20000 NPs to 100000 NPs in every cubic centimetre of atmosphere. Atmospheric nanoparticles have two emission sources. These are primary emissions and secondary emissions. Primary emissions have a direct source whilst secondary emitted nanoparticles are formed due to chemical reactions which occur in the atmosphere [21].

Some natural sources of nanoparticles include; volcanic eruptions, physical and chemical weathering of rocks, precipitation reactions and biological processes [22,23]. Man-made sources of nanoparticles include; industrial pollution, domestic pollution (e.g. cooking, vacuuming) and car exhaust fumes. Nanoparticles can grow after they have been released into the atmosphere through condensation of gaseous particles into solid particles or coagulation of small particles into larger particles. Nanoparticles which have been released into the atmosphere may remain for several years [24].

Zinc oxide is an inorganic compound with the formula ZnO. It is a white powder that is insoluble in water, and it is one of the most widely used groups of nanoparticles. From use as a paint formulation and ceramic manufacture, to its use as a protective sunscreen in skin and hair care products and as an additive in numerous materials and products including rubbers, plastics, ceramics, glass, cement, lubricants, paints, ointments, adhesives, sealants, pigments, foods, batteries, ferrites, fire retardants, and first-aid tapes. It occurs naturally as the mineral zincite, but most zinc oxide is produced synthetically. Zinc oxide crystalizes into two main nanoparticle forms; hexagonal wurtzite and cubic zinc blende. The wurtzite structure is most stable at ambient conditions and thus is most common. The manufactured zinc oxide nanoparticles used in this project are 20 nm in diameter and mimic those derived from vehicle catalytic converters [25].

Cerium oxide is an oxide of the rare earth metal, cerium. It is a pale yellow powder with the chemical formula CeO₂. It has wide applications ranging from uses in ceramics, to uses in sensitising photosensitive glass. It is also used as a catalyst and a catalyst support [27-29]. A buffer layer for superconductors; Coatings for infrared filters; colouring agents for plastics; Electrolyte and/or electrode materials for solid oxide fuel cells; Heat resistant alloy coatings; Infrared absorbents; Oxidation resistant coatings; Oxygen pumps; Oxygen sensors; Polishing media for electronic devices, glasses, and bearing balls; Sintering additives. The cerium dioxide nanoparticles used in this project are 8 nm in diameter and mimic those present in a diesel additive used in public service vehicles [18] **(FIGURE 3-5).**

This project used the 16HBE14o cell line which is epithelial cell line to investig
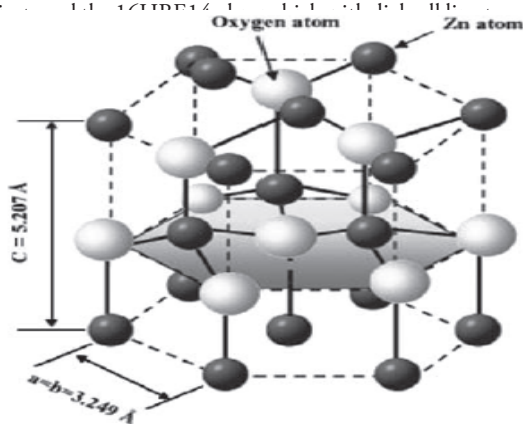
FIGURE 3. The hexagonal wurtzite structure model of ZnO. The tetrahedral coordination of Zn-O is shown atoms are shown as larger white spheres while the Zn atoms are smaller brown spheres [26]
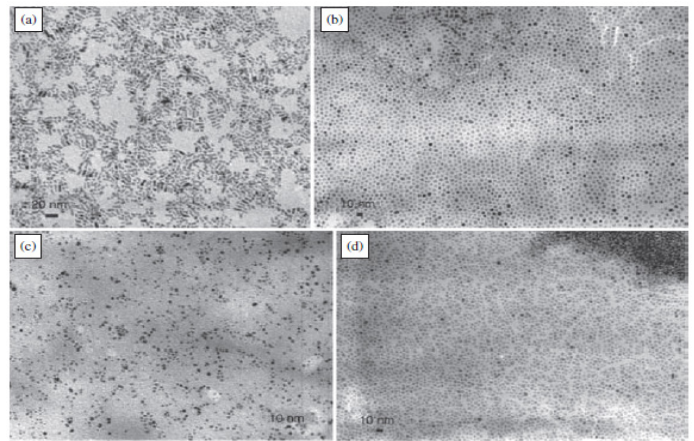
FIGURE 4. Transmission Electron Micrograph of Zinc Oxide Nanoparticles, a) Nanorods b), c), d) Nano disks [26]
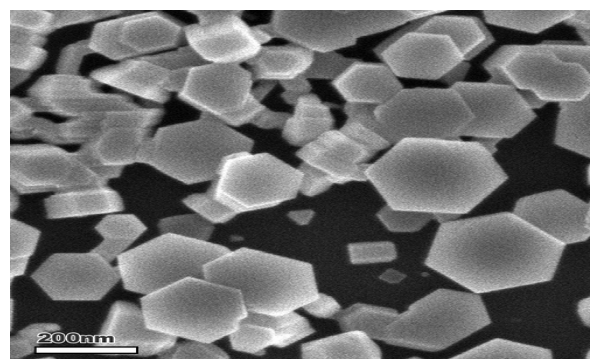
FIGURE 5. Scanning electron micrograph of zinc oxide nanoparticles [26]

the effect of zinc oxide (ZnO) and cerium dioxide (CeO₂) nanoparticles on bronchial epithelial cell functions. This cell line was obtained by viral transformation of normal bronchial epithelial cells obtained from a 1-year-old heart-lung transplant patient. The transformation was done with the hybrid virus, adeno-12-SV40 and was originally developed to study the chloride channel activity of the Cystic Fibrosis Transmembrane Conductance Regulator (CFTR) [30]. 16HBE14o cells have a cobblestone appearance in culture, they form functional tight junctions in culture and they show directional vectoral ion transport [31]. The cell line can be cultured submerged at a solid liquid interface or at an air liquid interface. When cells are cultured on collagen coated supports at an air-liquid interface, they retain very important properties of differentiated airway epithelial cells. These include the formation of tight junctions, directed regulated ion transport and crucial morphological features, including apical microvilli and cilia [32] **(FIGURE 6).**

The two types of cell death that nanoparticles could induce on the cell line are apoptosis (the process of programmed cell death, which could lead to blebbing, cell shrinkage, nuclear fragmentation, chromatin condensation and chromosomal DNA fragmentation) and necrosis/cytotoxicity (a process of traumatic cell death which leads to the generation of reactive oxygen species) **(FIGURE 7)**

This project addressed the hypothesis that exposure of the 16HBE14o bronchial epithelial cell line to nanoparticles will have significant detrimental effects on cell viability and also lead to an increase in pro inflammatory cytokine production by bronchial epithelial cells. IL-8 secretion will be used as an exemplar pro-inflammatory chemokine with IL-33 release being of interest due to it being both pro-inflammatory and an alarmin that has been implicated in asthma pathogenesis [7]. It is well established that asthmatic individuals are more sensitive to the deleterious effects of inhaled particulates and that the same may be true of exposure

(a)   **(b)**
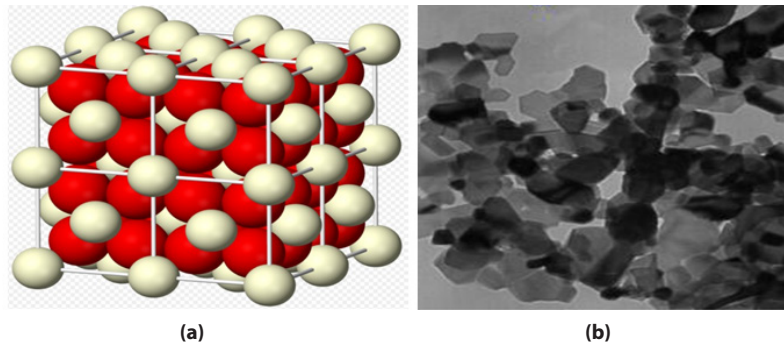
FIGURE 6 (a). 3-D structure of Cerium dioxide nanoparticle crystals; 6(b): Transmission electron micrograph of cerium dioxide nanoparticles [26]
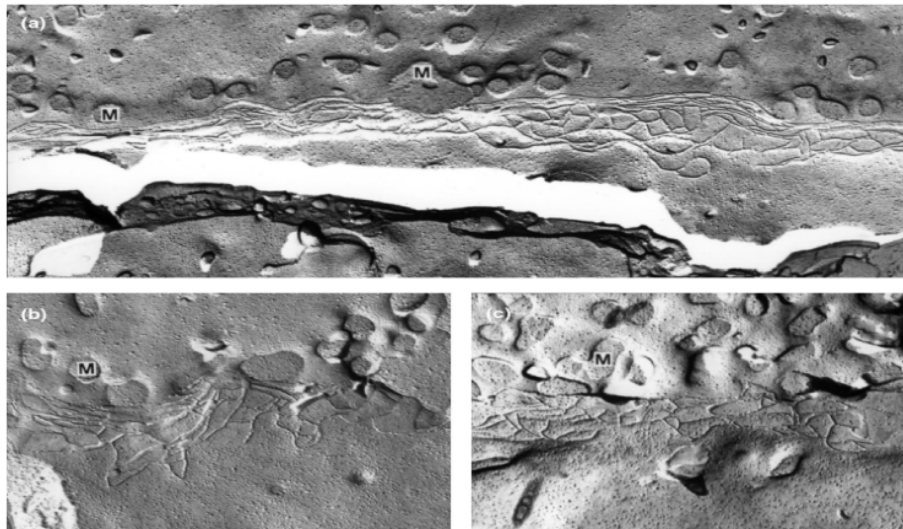
FIGURE 7. Freeze fracture electron microscopy showing tight junctional belts found in 16HBE14o cells [32]

to nanoparticles [33]. Nanoparticles present in the atmosphere could potentially cause airway injury, repair, and inflammation and promote re-activation of the EMTU with significant effects on both late onset non-atopic intrinsic asthma and early onset atopic asthma. The demonstration that nanoparticles have adverse effects on AEC and that children/adults with asthma are particularly susceptible will lead to further clinical studies of controlled inhaled nanoparticle challenges [34,35]. The ultimate impact will be to inform governmental nanoparticle policy, the motor vehicle and nanomaterial industries and potentially lead to changes within the automotive industry to reduce nanoparticle emissions, e.g. changes in alloys, fuel additives and catalytic converter design.

Aim

To determine the cytotoxic effect, the type of cell death induced and the pro inflammatory cytokine secretory phenotype of bronchial epithelial cells stimulated with nanoparticles.

Specifically, my aims were to:

• Investigate the cytotoxic effect of Zinc Oxide and Cerium dioxide nanoparticles on 16HBE14o Bronchial Epithelial Cells

• Investigate the type (if any) of cell death (apoptosis or necrosis) induced by both nanoparticles on 16HBE14o Bronchial Epithelial Cells

• Investigate the production of the pro inflammatory cytokines, IL-8 and IL-33 by 16HBE14o Bronchial Epithelial cells stimulated with Zinc Oxide and Cerium dioxide nanoparticles

Hypothesis

Based on the findings of Kim, Fazlollahi et al, 2010 and Sahu, Kannan et al, 2013, it was expected that zinc oxide nanoparticles will cause cytotoxicity

to 16HBE14o bronchial epithelial cells in a dose dependent manner [36,37]. Based on the findings of Srinivas A, Rao PJ et al, 2011 and Park, Choi et al, 2008, Cerium dioxide nanoparticles may cause cytotoxicity to 16HBE14o cells in a dose dependent manner [8,38].

Based on the findings of Sahu et al, 2013, increased zinc oxide nanoparticle concentration may lead to an increase in ROS production by bronchial epithelial cells [37]. Also based on the findings of Park et al, 2008, increased cerium dioxide nanoparticle concentration may result in increased ROS production by 16HBE14o cells [41].

Based on the findings of Lu Y et al, 2013, increased zinc oxide nanoparticle concentration may lead to an increase in IL-8 expression and production by bronchial epithelial cells [39]. Furthermore, based on the findings of Pace et al, 2014, increased zinc oxide and cerium dioxide nanoparticle concentration may result in increased IL-33 secretion 16HBE14o cells [40].

Materials

The objective was to investigate the cytotoxic effect and the pro inflammatory cytokine secretory phenotype of 16HBE14o bronchial epithelial cells stimulated with zinc oxide and cerium dioxide nanoparticles. This cell line was therefore cultured using several vessels depending on the type of experiment or assay to be performed. Initial culture used a T75, a 96 well plate was used for the cytotoxicity assay and ELISA, a 12 well plate for nanoparticle exposures and a chamber slide for the immunohistochemistry analysis.

▪ **Cell line**

The human bronchial epithelial cell line used (16HBE14o-) was obtained from Gruenert Laboratory, University of California, Mount Zion Cancer Center, San Francisco, USA at a passage number of P2:49

▪ Culture media

The Minimum Essential Medium Eagle (MEM) media used contains 292 g/L L-Glutamine, 1 g/L Glucose, and 2.2 g/L NaHCO$_3$. 450 ml of MEM was supplemented with 50 ml Fetal Calf Serum (Product number: F2442 SIGMA), 5 ml (100x) Penicillin/Streptomycin (Product Number: CCFGK004) and 5 ml (200 mM, 100 ml) L-Glutamine (Product Number: 25030081), all purchased from Sigma-Aldrich Company Ltd. Dorset. UK (TABLE 1).

Methods

▪ Cell culture

A T75 flask containing ~85% confluent 16HBE14o bronchial epithelial cells were obtained. These were cultured in fibronectin coated T75 flasks using the culture media described above. They were then seeded into 96 and 12 well plates. Media was refreshed every 48 hours to 72 hours and the cells were passaged into newly coated vessels once they reached ~80% confluence.

Cells were incubated in a Sanyo Incubator within a humidified atmosphere composed of 95% air: 5% CO$_2$ at a temperature of 37℃.

All cell culture procedures were conducted in sterile conditions in a Laminar Flow Cabinet (FIGURE 8).

▪ Acid phosphatase assay for cytotoxicity testing

Concentration 16HBE14o cells were dosed with an increasing concentration of zinc or cerium dioxide nanoparticles with media as a negative control and triton x as a positive control.

150 μl cell suspensions were seeded into 90 wells of fibronectin coated 96 well plates at a seeding density of 1 x 10⁴ cells/cm²/well. 6 wells were left blank. The plates were then cultured to ~80% confluence for 96 hours. 100 μl of media (base control)/5% Triton X-100 (positive control)/TNFα and IL-1β/Zinc Oxide and Cerium dioxide nanoparticles were added to the relevant wells as shown in the template in the below TABLE 2. These were done in triplicates twice so that an n=6 dosing regimen was achieved for each stimulant and concentration utilised on each plate. The plates were

then incubated at 37℃ for 24 hours. 100μl acid phosphatase substrate solution (acid phosphatase buffer + P-nitrophenol phosphate tablets) was added to each well and incubated for 2 hours at 37℃ in the dark. The reaction was stopped with 50 μl 0.5M NaOH and absorbance of each well read on a spectrophotometer at 405 nm single wavelength. A graph of percentage viability of 16HBE14o cells stimulated with varying zinc and cerium dioxide nanoparticle concentration was constructed. The entire procedure was repeated and an n=2 graph was generated for percentage viability of both zinc oxide and cerium dioxide (TABLE 2).

▪ Dosing 12 well plate with nanoparticles

750μl cell suspension was seeded into all the wells of a fibronctin coated 12 well plate at a seeding density of 1 x 10⁴ cell/cm²/well. Then they were cultured to ~80% confluence for 96 hours. 500 μl of media, TNF-α/IL-1β and increasing concentrations of Zinc oxide and Cerium dioxide nanoparticles were added to the relevant wells as shown in the template below. The plates were incubated for approximately 24 hours before collection of supernatants and preparation of cell lysates. This procedure was performed on 4 x 12 well plates (TABLE 3).

▪ Collection of supernatants and preparation of cell

EXPLANT CULTURE

Tissue at solid-liquid interface; cells migrate to form outgrowth
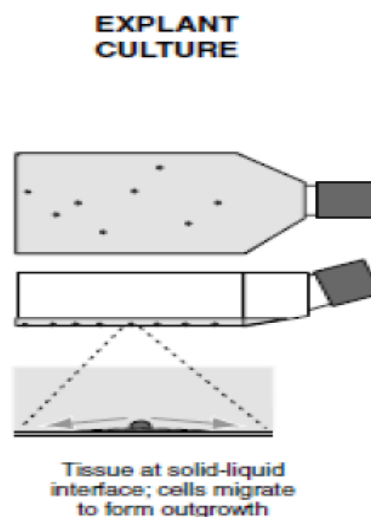
FIGURE 8. Sterile conditions in a laminar flow cabinet

TABLE 1. Reagents, chemicals & major technique kits	
Phosphate Buffer Saline Tablets	GibcoTM by Life Technologies Ltd
Fibronectin Coating Solution	Sigma-Aldrich Company Ltd
Trypsin	PAA Laboratories
Trypan Blue (Product number: T6146 Sigma)	Sigma-Aldrich Company Ltd
Triton X (Product number: N150 Sigma)	Sigma-Aldrich Company Ltd
TNFα and IL-1β	R&D systems
p-Nitrophenol Phosphate tablets (Product Number: 241326 Aldrich)	Sigma-Aldrich Company Ltd
Complete mini protease Inhibitor tablet	Roche Diagnostics
Haemocytometer	Hawksley Medical and Laboratory equipment
The T75cm² flasks	Nunc, Fisher Scientific UK Ltd
12 well plates	Nunc, Fisher Scientific UK Ltd
96 well plates	Nunc, Fisher Scientific UK Ltd
Zinc oxide (20 nm)	University of Birmingham
Cerium dioxide (8 nm)	University of Birmingham
Coomassie (Bradford) Assay Kit	Fisher Scientific - laboratory supplies & equipments
IL-8 ELISA kit	Bio Legend
IL-33 ELISA kit	Affymetrix eBioscience eBioscience
Immunocytochemistry anti-cytokeratin 19 antibody	Abcam
DAB kit	Vector Laboratories
Apoptosis assay kit	Millipore Corporation

TABLE 2. Acid phosphatase assay for cytotoxicity testing

	1	2	3	4	5	6	7	8	9	10	11	12
A	Ce 100	Ce 100	Ce 100	Zn 100	Zn 100	Zn 100	Ce 100	Ce 100	Ce 100	Zn 100	Zn 100	Zn 100
B	Ce 50	Ce 50	Ce 50	Zn 50	Zn 50	Zn 50	Ce 50	Ce 50	Ce 50	Zn 50	Zn 50	Zn 50
C	Ce 25	Ce 25	Ce 25	Zn 25	Zn 25	Zn 25	Ce 25	Ce 25	Ce 25	Zn 25	Zn 25	Zn 25
D	Ce 10	Ce 10	Ce 10	Zn 10	Zn 10	Zn 10	Ce 10	Ce 10	Ce 10	Zn 10	Zn 10	Zn 10
E	Ce 5	Ce 5	Ce 5	Zn 5	Zn 5	Zn 5	Ce 5	Ce 5	Ce 5	Zn 5	Zn 5	Zn 5
F	Ce 2.5	Ce 2.5	Ce 2.5	Zn 2.5	Zn 2.5	Zn2.5	Ce 2.5	Ce 2.5	Ce 2.5	Zn 2.5	Zn 2.5	Zn2.5
G	M	M	M	TRITON X	TRITON X	TRITON X	M	M	M	TRITON X	TRITON X	TRITON X
H	TNF/IL1b	TNF/IL1b	TNF/IL1b	NO CELLS	NO CELLS	NO CELLS	TNF/IL1b	TNF/IL1b	TNF/IL1b	NO CELLS	NO CELLS	NO CELLS

TABLE 3. Dosing 12 well plate with nanoparticles

	1	2	3	4
A	MEDIUM	TNFα/IL1β	Zn 2.5	Zn 5
B	Zn 10	Zn 25	Zn 50	Zn 100
C	Ce 10	Ce 25	Ce 50	Ce 100

lysates

Supernatants from each of the wells of the 12 well plates were collected into eppendorf tubes. They were centrifuged at 1100 rpm for 5 minutes at 4°C and stored at -20°C prior to performing ELISA for cytokine detection. Similarly, 500 μL lysing buffer was added to each well and the plate agitated for 5 minutes. The adherent cells were scraped using a scraper and the lysates removed into labelled Eppendorf tubes. These were then centrifuged at 2000 rpm for 5 minutes at 4°C and stored at -20°C prior to analysis for protein content. A schematic of this procedure is shown in **FIGURE 9**.

▪ Bradford assay for protein quantification

25 μL of sample lysates and 25 μL of increasing protein standard concentrations ranging from 0 μg/ml to 1000 μg/ml were added to appropriate wells of a 96 well plates in duplicate. 200 μL Bradford reagent was then added prior to incubating the plates at room temperature for 10 minutes. The absorbance at 595 nm using a 4 parameter logistic regression for curve fit was used to estimate the protein concentration in each of the cell lysate. These will be used to standardize the cytokine concentration, if any, found in each of the corresponding wells of the 12 well plates.

▪ ELISA

An enzyme linked immunosorbent assay procedure was carried out to detect and quantify, if any, the amount of IL-8 and IL-33 present in each of our supernatant samples. A stock concentration of IL-8 capture antibody was diluted and 100 μL of this was used to coat each well of two 96 well plates, 24 hours before the beginning of the procedure. The Plates were washed and 200 μL assay diluent was added to block non-specific binding and reduce background. A serial dilution of the IL-8 standard was performed and 100 μL of this was added in duplicates to specific wells as shown in the schematic below. 100 μL supernatant samples from the blue eppendorfs were then added in duplicates. The plates were incubated and washed. 100 μL detection antibodies were added to each well before another incubation step. Plates were washed again, than 100 μL diluted Avidin-HRP solution was added to each well. After the final wash step, 100 μL substrate solutions C was added to each well and the plates were incubated in the dark for 15 minutes before 100 μL of a stop solution was added. The absorbance was read at 450 nm and 570 nm using a plate reader within 30 minutes of completing the procedure. The absorbance at 570 was then subtracted from the absorbance at 450 nm. A standard curve was generated using the absorbance measurements of the IL-8 standards and the IL-8 concentration present in each duplicate sample was estimated and averaged. The IL-33 kit utilized was manufactured pre-coated with capture antibody. 50 μL sample diluent was added to each well of the 96 well plates. A serial dilution of the IL-33 standard was prepared and added in duplicate to relevant wells of the plate as shown in the schematic below. 50 μL calibrator diluent was added to the blank wells and 50 μL of samples were added in duplicate to the sample wells. The plates were incubated and washed prior to adding 100 μL Biotin-conjugate into all the wells. The plates were incubated and 100 μL Streptavidin-HRP was added into all the wells and incubated again. 100 μL TMB substrate solution was added into the entire well and incubated. Then 100 μL stop solution was added into all the wells before an absorbance reading was carried out at 450 nm. A standard curve was generated using the IL-33 standards and the amount of IL-33 present in the duplicate sample wells estimated and averaged (**TABLE 4**).

▪ Apoptosis assay

16HBE14o cells were cultured to ~80% confluence in a 96 well plate prior to dosing with increasing concentrations of zinc oxide and cerium dioxide nanoparticles for 24 hours before commencing the assay. The plate was then centrifuged and the cells fixed with 80% methanol in PBS. The pate was dried in an incubator, than 50 μL form amide was added to each well and incubated at room temperature. Plates were heated to 75°C in a water bath for 10 minutes then cooled in a refrigerator for 5 minutes. 100 μL SI nuclease was then added to the negative control wells whilst 10 μL ssDNA was added to wells with no cells in them as a positive control. After a rinsing step, 200 μL of 3% nonfat dry milk was added to all the wells and incubated for 1 hour at 37°C. 100 μL antibody mixtures was then added into all the wells, incubated for 30 minutes, the 100 μL ABTS solution was added and plate incubated until a colour change is seen. The reaction was stopped by adding 100 μL stop solution into each well and absorbance read in a standard microplate reader at 405 nm.

▪ Reactive oxygen species assay

16HBE14o cells were cultured to ~80% confluence on a flat bottomed 96 well plates. They were then dosed with increasing concentrations of zinc oxide and cerium dioxide nanoparticles for a period of 24 hours before commencing the assay. 100 μL of a pre-prepared carboxy-DCFDA probe (50 μM H2DCFDA in PBS) was added to all the wells containing nanoparticle concentrations. 60 minutes, 37°C incubation in the dark then followed. Then the wells were washed with PBS. A1 hour incubation with H$_2$O$_2$ was used as a positive control. Fluorescence at 530 nm was measured using a spectrophotometer.

▪ Immunocytochemistry

16HBE14o cells were cultured to ~80% confluence in 12 well plates. Then they were fixed with 200 μl Methanol:Acetone mix (1:1) and placed in the fridge prior to staining. Designated well were washed and incubated with 200μl protein blocking solution. Then the positively stained wells
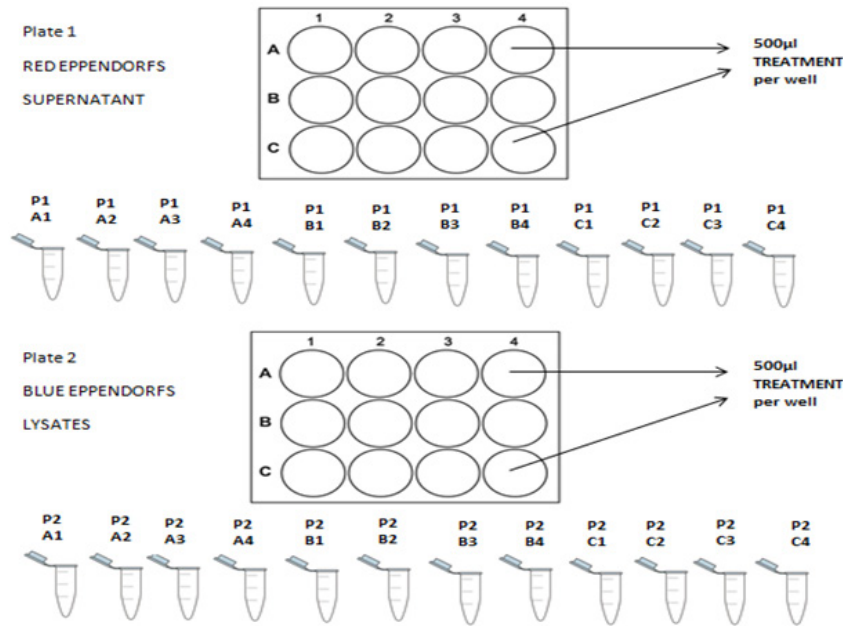
FIGURE 9. Preparation of cell lysates

TABLE 4. Dosing 12 well plate with nanoparticles								
	1	**2**	**3**	**4**	**5**	**6**	**7**	**8**
A	1000	1000	A1	A1	C1	C1	B1	B1
B	500	500	A2	A2	C2	C2	B2	B2
C	250	250	A3	A3	C3	C3	B3	B3
D	125	125	A4	A4	C4	C4	B4	B4
E	62.5	62.5	B1	B1	A1	A1	C1	C1
F	31.3	31.3	B2	B2	A2	A2	C2	C2
G	15.6	15.6	B3	B3	A3	A3	C3	C3
H	0	0	B4	B4	A4	A4	C4	C4

were incubated with primary antibody (monoclonal anti-cytokeratin -19) for one hour while the negatively stained control was incubated with PBS tween. Following another washing step, both positive and negative control wells were incubated with HRP secondary antibody for 30 minutes at room temperature. Then, another washing step and the addition of a few drops of DAB buffer (5 ml H$_2$0, 2 drops of buffer stock solution, 4 drops of DAB stock solution, 2 drops of H$_2$O$_2$ stock solution from DAB kit) The plate was then incubated for 5 minutes until a colour development is see. Photos were then taken using an EVOX microscope.

▪ **Statistical analysis**

The results of the cytotoxicity tests, ELISA, ROS assay and apoptosis assay are presented as mean +/- Standard Deviation (SD) of between two - six separate samples or experiments. Using the SPSS (Statistical Package for the Social Sciences) software, the values of the IL-8 and IL-33 concentration pg/μg protein at each nanoparticle concentration produced were compared to media alone and significance was evaluated and presented using a t-test.

Results

▪ **Cell culture**

As can be seen clearly from **FIGURE 10** below, the cell number increased linearly with time in culture with a cobblestone appearance by 16HBE140 visible **(FIGURE 10 b, c and d)**.

▪ **Immunocytochemistry**

FIGURE 11 shows the result of the immunocytochemical analysis performed on the cell line. Monoclonal anti-cytokeratin 19 antibodies

were used to positively stain for the presence of intermediate filament proteins which maintain the structural integrity of all epithelial tissue. **FIGURE 11(a)** is a light blue transparent result as a negative control was used for the staining. **FIGURE 11(b)** is dark brown. This is a positive result demonstrating the epithelial nature of 16HBE14o cells.

▪ **Cytotoxicity - Acid Phosphatase assay**

The lowest overall percentage viability observed with the positive control, triton x (0.5%) as expected. The range (difference between the highest and lowest percentage viability) of percentage viability observed with CeO$_2$ nanoparticles utilised is 120% to 92% (28%) but these changes were not significant **(FIGURE 12)**.

From **FIGURE 13**, percentage viability of the cells increased with ZnO concentration from 2.5 μg/ml (88%) to 10 μg/ml (116%). The highest percentage viability is observed at the ZnO nanoparticle concentration of 10 μg/ml (116%). A steady decrease in percentage viability is then observed between ZnO nanoparticle concentrations of 25 μg/ml (93%) and 100 μg/ml (12%). The percentage viability associated with TNFα/IL1β is 104%. The lowest overall percentage viability is observed with the positive control triton x (0.5%).

Compared to CeO$_2$ nanoparticles, ZnO nanoparticles have a much more cytotoxic effect on the 16HBE14o cell line. The range of percentage viability observed with CeO$_2$ is 28% whilst the range observed with ZnO is 104%.

▪ **ELISA**
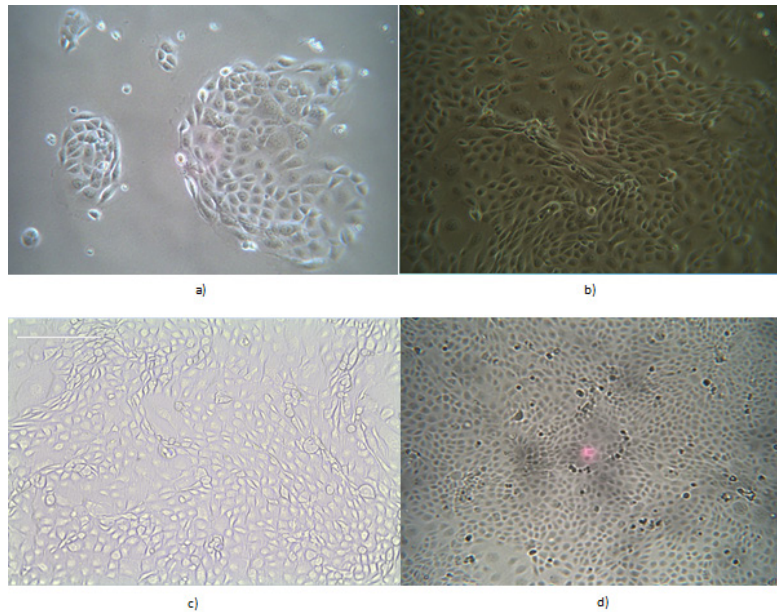
FIGURE 10. Photomicrographs of cultured 16HBE14o bronchial epithelial cells at different time points after seeding at a density of 1 x 104 cells/cm³ in a T75 flask. These photos were taken using an Infinity 2 camera attached to a high resolution inverted light microscope. (a) Day 2 after seeding. X20; (b) Day 5 after seeding. X20; (c) Day 7 after seeding. X20; (d) Day 14 after seeding. X20

(a)   **(b)**
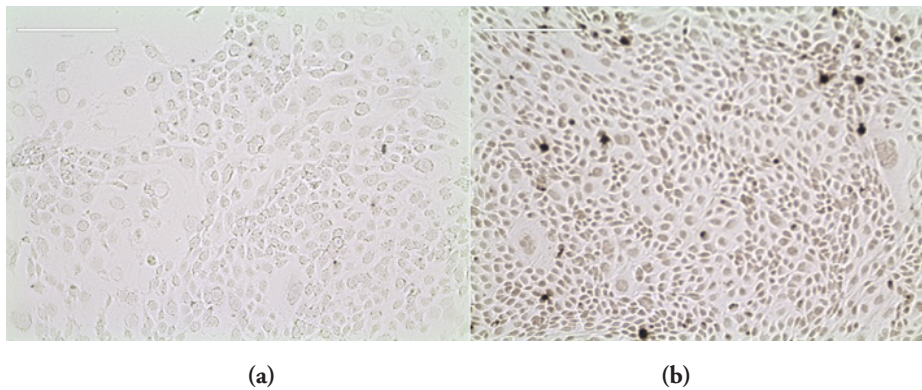
FIGURE 11. Immunocytochemistry analysis of 16HBE14o bronchial epithelial cells. Monoclonal Anti-Cytokeratin 19 antibody (against keratin 19, a member of the intermediate filament proteins responsible for the structural integrity of epithelial cells) was used to positively stain the epithelial cells. PBS was used as a negative control. (a) On the left is light blue. This is a negative result; (b) On the right is dark brown. This is a positive result. Pictures were taken using an EVOX microscope. X10
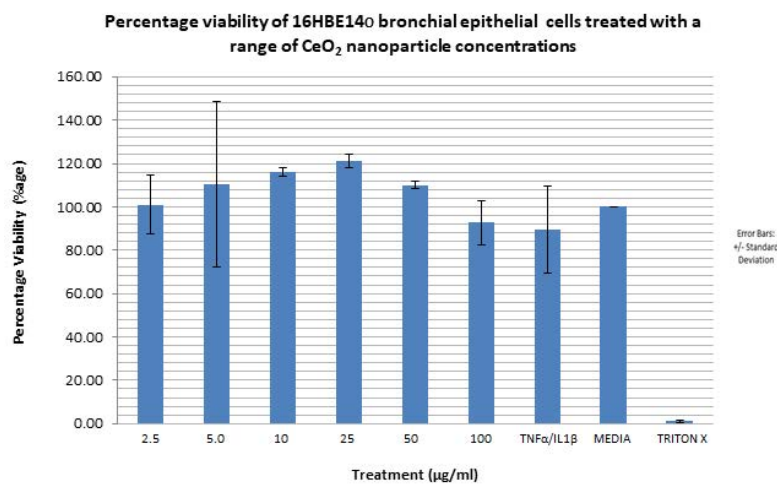
FIGURE 12. Bar graph showing the percentage viability of 16HBE14o bronchial epithelial cells treated with increasing concentrations of 8nm cerium dioxide nanoparticles for a period of 24 hours. Cerium dioxide nanoparticle concentration range utilised: 2.5 µg/ml to 100 µg/ml. Viability is expressed as a percentage of the mean optical density (from 6 samples of the same nanoparticle concentration) associated with different nanoparticle concentration against the optical density associated with the positive control; media alone. The media has a percentage viability of 100%.The bar graph represents an average of two independent acid phosphatase cytotoxicity experiments performed under the same conditions. N=2. Error bars represent mean percentage viability +/- standard deviation. Triton X was used as a negative control.

Percentage Viability of 16HBE14o bronchial epithelial cells treated with a range of ZnO nanoparticle concentrations
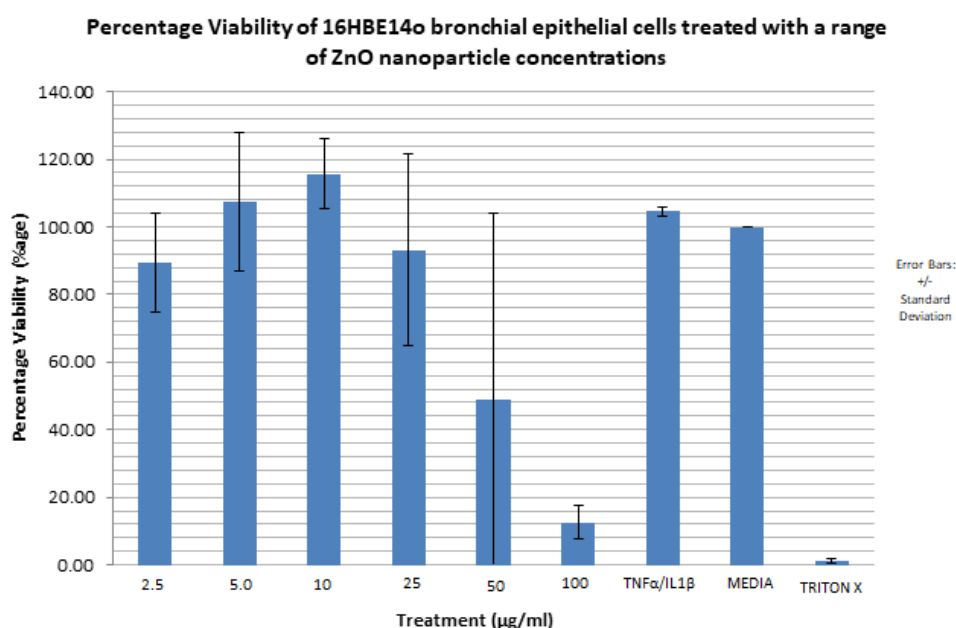
FIGURE 13. Bar graph showing the percentage viability of 16HBE14o bronchial epithelial cells treated with increasing concentrations of 20 nm zinc oxide nanoparticles for a period of 24 hours. Zinc oxide nanoparticle concentration range utilised: 2.5 µg/ml to 100 µg/ml. Viability is expressed as a percentage of the mean optical density (from 6 samples of the same nanoparticle concentration) associated with different nanoparticle concentration against the optical density associated with the positive control; media alone. The media has a percentage viability of 100%.The bar graph represents an average of two independent acid phosphatase cytotoxicity experiments performed under the same conditions. N=2. Error bars represent mean percentage viability +/- standard deviation. Triton X was used as a positive control.

TABLE 5. Table showing the IL 8 concentration pg/µg protein produced into culture supernatant by 16HBE14o bronchial epithelial cells dosed with increasing zinc oxide and cerium dioxide nanoparticle concentrations. Each value represents the IL-8 concentration produced divided by the amount of protein present in that well. The mean represents the average of four independent samples (P1 - P4) and is used to construct the bar graph representative of these values. The P value describes how statistically significant the IL-8 produced at the different nanoparticle concentration is compared with the media (no treatment). When p > 0.05, this is ns (not significant). When p < 0.05, this is * (significant). When p < 0.01, this is ** (very significant). When p < 0.001, this is *** (extremely significant)

	Mean	S.D	T	p	significance
Medium	29.1093375	18.9800947			
TNFα/IL1β	43.0382411	8.66145617	-1.509	0.228	not significant
Zn 2.5	32.0065759	6.70923295	-0.3	0.784	not significant
Zn 5	35.4340682	15.5426182	-0.806	0.479	not significant
Zn 10	36.2830624	13.6571261	-1.862	0.16	not significant
Zn 25	41.7690474	31.9869995	-0.979	0.4	not significant
Zn 50	22.363885	15.6008226	0.908	0.431	not significant
Zn 100	22.9324132	4.61684993	0.653	0.56	not significant
Ce 10	23.4208554	17.90994	0.998	0.392	not significant
Ce 25	24.6580865	20.0880152	0.736	0.515	not significant
Ce 50	22.6171984	20.4140539	1.048	0.372	not significant
Ce 100	25.5392815	15.0774595	0.395	0.719	not significant

TABLE 5 above shows the statistical significance in form of a t-test of IL-8 production pg/µg protein at each Zinc and Cerium nanoparticle concentration compared to media. All the values are not significant according to the t test. This is also confirmed by the error bars on the graph in **FIGURE 13** which reflect the standard deviation values.

▪ The cytotoxicity assay of ZnO on 16HBE14o cells

The same range of nanoparticle concentrations from the cytotoxicity assays were used to dose the cells. Supernatants were collected and an ELISA was performed to measure the secretion of IL-8 and IL-33. From the IL-8 ELISA results shown in **FIGURE 14** above, the greatest amount of IL-8 pg/µg protein produced was seen with TNFα/IL1β. This was expected as TNFα/IL1β is a pro inflammatory cytokine and was added as a positive control. IL-8 production was variable from 32 pg/µg proteins to 42 pg/

µg protein as ZnO nanoparticle concentration increased from 2.5 µg/ml to 25 µg/ml with a sharp decrease at 50µg/ml ZnO (22 pg/µg protein). A slight increase thereafter is then seen at 100 µg/ml to 23 pg/µg protein. ZnO nanoparticles had a measurable but non-significant effect on IL-8 production of the 16HBE14o cell line.

With regards to the CeO$_2$ nanoparticles, the IL-8 production pg/µg protein was negative. This suggests that Cerium dioxide nanoparticles have no effect on IL-8 secretion in this cell line.

TABLE 6 above shows IL-33 production pg/µg protein at each Zinc and Cerium nanoparticle concentration compared to media. All the values are not significant according to the t test. This is also confirmed by the wide and overlapping error bars on the graph in **FIGURE 15** which reflect the standard deviation values. The amount of IL-33 produced by the

IL-8 production pg per µg protein of 16HBE14o cells treated with Zinc and Cerium nanoparticles
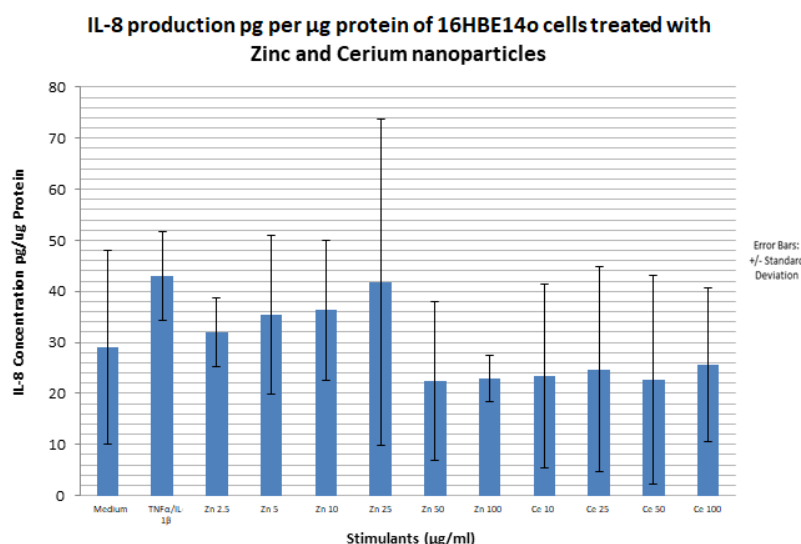
FIGURE 14. Bar graph showing IL-8 secretion into media supernatant per µg protein of 16HBE14o bronchial epithelial cells treated with media alone, TNFα/IL1 β, increasing concentrations of 40 nm zinc oxide and 8 nm cerium dioxide nanoparticles for a period of 24 hours. Zinc oxide nanoparticle concentration range utilised: 2.5 µM to 100 µM. Cerium dioxide nanoparticle concentration utilised: 10 µM to 100 µM. The bar graph represents an average of four independent 12 well plate samples treated with nanoparticles. N=4. Error bars represent mean IL 8 concentration in pg per µg protein of 16HBE14o cells +/- standard deviation. The P value describes how statistically significant the IL-8 produced at the different nanoparticle concentration is compared with the media (no treatment). When p > 0.05, this is ns (not significant). When p < 0.05, this is * (significant). When p < 0.01, this is ** (very significant). When p<0.001, this is *** (extremely significant). IL-8 ELISA Kit sensitivity: 8pg/ml.

TABLE 6. Table showing the IL 33 concentration pg/µg protein produced into culture supernatant by 16HBE14o bronchial epithelial cells dosed with increasing zinc oxide and cerium dioxide nanoparticle concentrations. Each value represents the IL-33 concentration produced divided by the amount of protein present in that well. The mean represents the average of four independent samples (P1-P4) and is used to construct the bar graph representative of these values.

	Mean	S.D	T	p	Significance
Medium	0.0028008	0.0056016	1	0.391	
TNFα/IL1β	0	0	1	0.391	not significant
Zn 2.5	0	0	1	0.391	not significant
Zn 5	0	0	1	0.391	not significant
Zn 10	0	0	1	0.391	not significant
Zn 25	0	0	1	0.391	not significant
Zn 50	0	0	1	0.391	not significant
Zn 100	0.0003085	0.000617	1	0.391	not significant
Ce 10	0	0	1	0.391	not significant
Ce 25	0	0	1	0.391	not significant
Ce 50	0	0	1	0.391	not significant
Ce 100	0.0011097	0.0022195	0.506	0.647	not significant

media, 100 µg/ml Zinc oxide and 100µg/ml cerium dioxide are below the sensitivity of the IL-33 ELISA kit 0.2 pg/ml (**FIGURE 15**).

▪ ROS assay

A ROS assay and an apoptosis assay were performed using similar nanoparticle concentrations used to dose the cells for the cytotoxicity assay and IL-8 or IL-33 secretion. **FIGURE 16** shows the result of the ROS assay for 16HBE14o cell line dosed with increasing cerium dioxide nanoparticle concentration. H$_2$O$_2$ is used as a positive control as it is known to induce production of ROS in epithelial cells. Percentage ROS production is calculated in proportion to the ROS produced in relation to the positive control, H$_2$O$_2$. The trend shown is that there is significant ROS production at the low CeO$_2$ nanoparticle concentrations and less ROS production at the higher nanoparticle concentrations apart from 25 µg/ml nanoparticle concentrations. The positive control, H$_2$O$_2$ failed to induce significant ROS production on the 16HBE14o cell line. They are presented in the **TABLE 7**.

FIGURE 17 shows the result of the ROS assay for 16HBE14o cells dosed

with increasing ZnO nanoparticle concentration. Similar to the percentage ROS production observed for 16HBE14o cells dosed with CeO$_2$ nanoparticles, the percentage ROS production observed for cells dosed with ZnO nanoparticles is more significant at the low ZnO nanoparticle concentrations than at the higher concentrations. They are presented in the **TABLE 8**.

▪ Apoptosis assay

An apoptosis assay was next performed with increasing cerium dioxide nanoparticle concentration. ssDNA was utilised as a positive control and S1 nuclease as a negative control. The percentage apoptosis observed for each cerium dioxide nanoparticle concentration are presented in the **TABLE 9**.

The highest percentage apoptosis, 3 7% is observed with the lowest CeO$_2$ nanoparticle concentration utilised i.e. 1.25 µg/ml. The lowest nanoparticle associated percentage apoptosis observed is associated with 50 µg/ml CeO$_2$ at 12%. The lowest overall percentage apoptosis is observed with the negative control, S1 nuclease at 4%, as expected. The highest
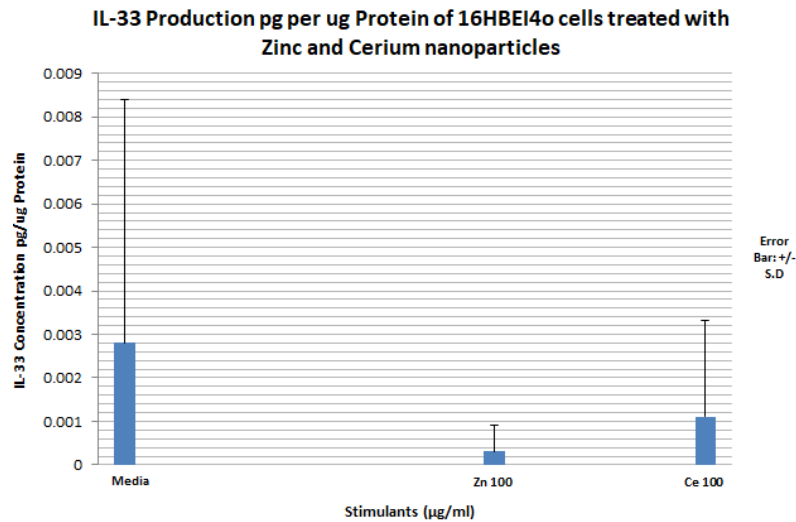
FIGURE 15. Bar graph showing IL-33 secretion (pg) into media supernatant per μg protein of 16HBE14o bronchial epithelial cells treated with media alone, TNFα/IL1 β, increasing concentrations of 20nm zinc oxide and 8 nm cerium dioxide nanoparticles for a period of 24 hours. Zinc oxide nanoparticle concentration range utilised: 2.5μg/ml to 100μg/ml. Cerium dioxide nanoparticle concentration utilised: 10 μg/ml to 100 μg/ml. The bar graph represents an average of four independent 12 well plates samples treated with nanoparticles. N=4. Error bars represent mean IL 33 concentration in pg per μg protein of 16HBE14o cells +/- standard deviation. IL-33 ELISA Kit sensitivity: 0.2 pg/ml
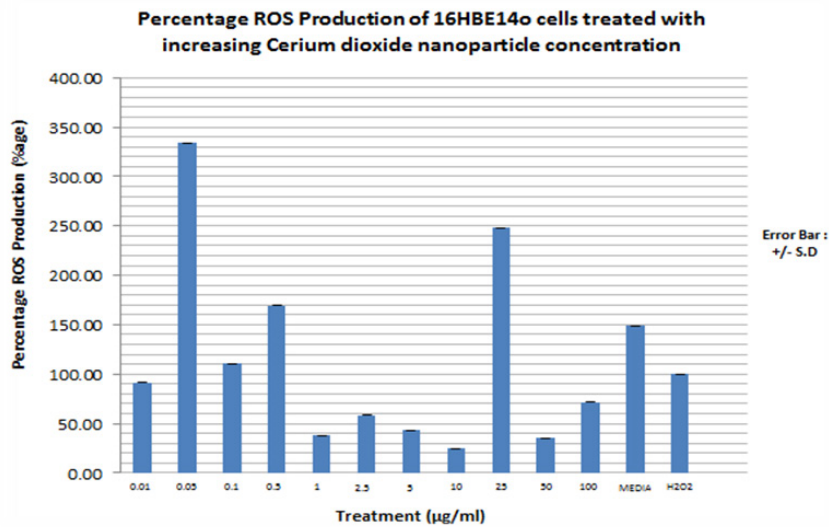
FIGURE 16. Bar graph showing the percentage total free radical production by 16HBE14o bronchial epithelial cells dosed with increasing cerium dioxide nanoparticle concentrations. Carboxy-DCFDA is used as a probe to detect cellular free radical formation. Media alone is used as a negative control. H$_2$O$_2$ (150μM, 1 hour) is used as a positive control as it is known to induce intracellular oxidative stress. Fluorescence at 530nm is measured on a spectrophotometer. The bar graph represents an average of triplicate values of each nanoparticle concentration used to dose the cells. N=3. These values represent the maximum rate of reaction at which ROS are produced

TABLE 7. The positive control, H$_2$O$_2$ failed to induce significant ROS production on the 16HBE14o cell line.	
CeO$_2$ Conc^n (μg/ml)	Percentage ROS Production (%)
0.01	90
0.05	335
0.1	110
0.5	170
1	40
2.5	60
5	45
10	25
25	250
50	35
100	70
Media	150
H$_2$O$_2$ (+ve control)	100

Percentage ROS Production of 16HBE14o cells treated with increasing Zinc Oxide nanoparticle concentration
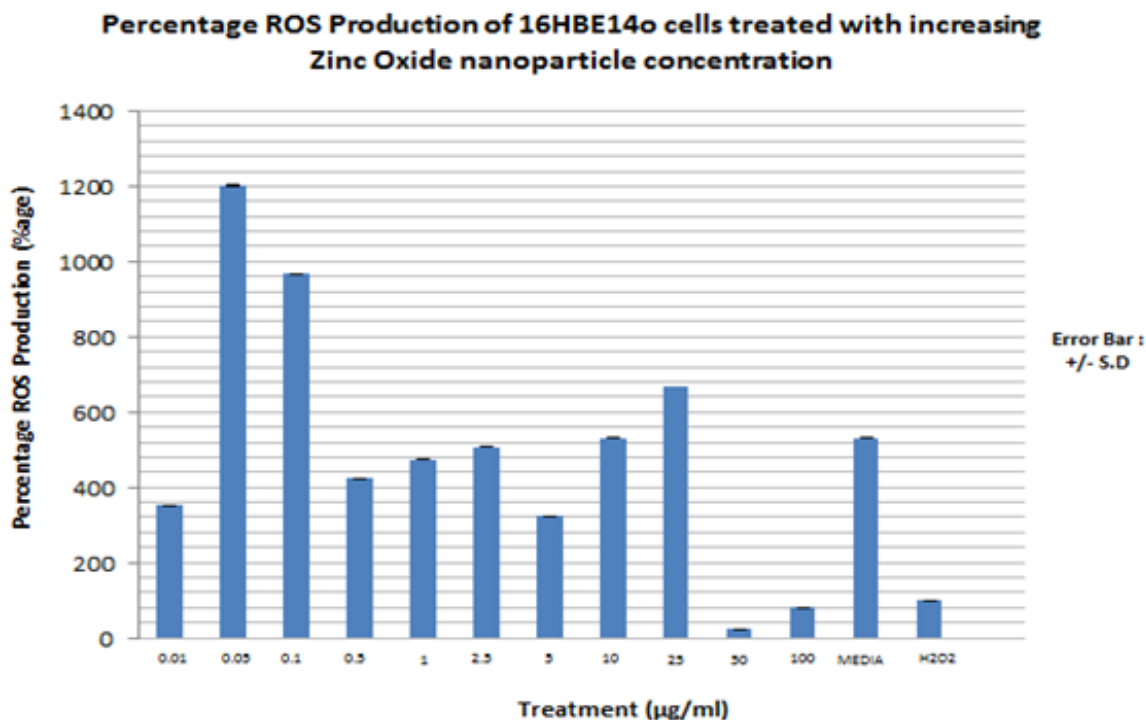
FIGURE 17. Bar graph showing the percentage total free radical production by 16HBE14o bronchial epithelial cells dosed with increasing cerium dioxide nanoparticle concentrations. Carboxy-DCFDA is used as a probe to detect cellular free radical formation. Media alone is used as a negative control. H$_2$O$_2$ (150 µM, 1 hour) is used as a positive control as it is known to induce intracellular oxidative stress. Fluorescence at 530nm is measured on a spectrophotometer. The bar graph represents an average of triplicate values of each nanoparticle concentration used to dose the cells. N=3. These values represent the maximum rate of reaction at which ROS are produced.

TABLE 8. The percentage ROS production observed for each ZnO concentration	
ZnO Conc^n (µg/ml)	**Percentage ROS Production (%)**
0.01	360
0.05	1200
0.1	960
0.5	420
1	480
2.5	500
5	320
10	520
25	680
50	30
100	80
Media	520
H$_2$O$_2$(+ve control)	200
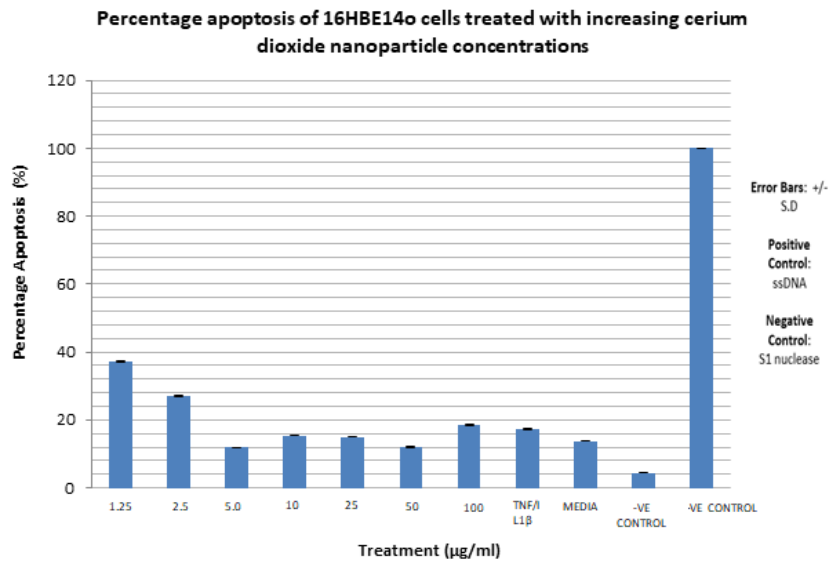
FIGURE 18. Bar graph showing the percentage apoptosis of 16HBE14o bronchial epithelial cells dosed with increasing cerium dioxide nanoparticle concentrations. SI nuclease is used as a negative control. ssDNA is used as a positive control. Absorbance at 405 nm, measured on a spectrophotometer is used to quantify cell death. Error bars indicate percentage apoptosis +/- standard deviation. The bar graph represents an average of duplicate values of each nanoparticle concentration used to dose the cells. N=2. These values represent the average rate of reaction at which ROS are produced.

TABLE 9. The percentage apoptosis observed for each cerium dioxide nanoparticle concentration	
CeO$_2$ Conc^n (µg/ml)	Percentage Apoptosis (%)
1.25	37
2.5	26
5	12
10	16
25	16
50	12
100	18
TNFα/IL1β	17
MEDIA	14
-VE CONTROL	4
+VE CONTEOL	100
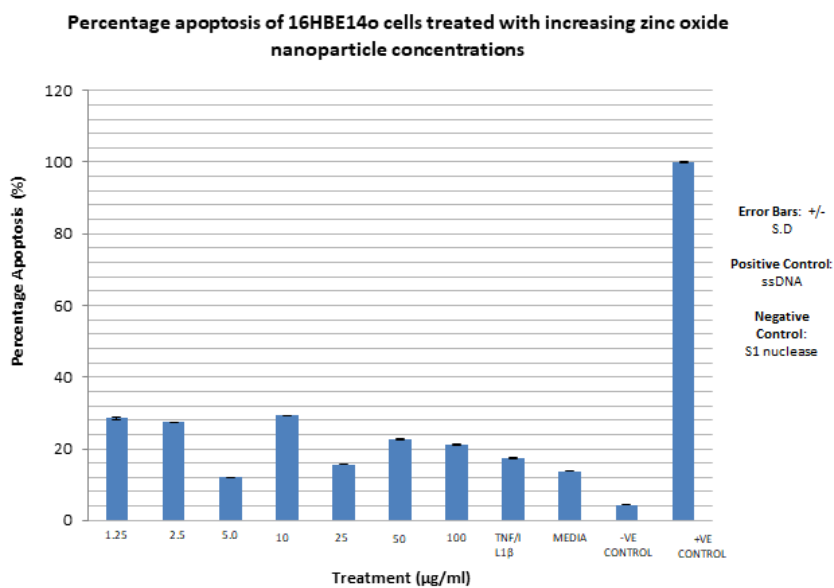
FIGURE 19. Bar graph showing the percentage apoptosis of 16HBE14o bronchial epithelial cells dosed with increasing zinc oxide nanoparticle concentrations. SI nuclease is used as a negative control. ssDNA is used as a positive control. Absorbance at 405 nm, measured on a spectrophotometer is used to quantify cell death. Error bars indicate percentage apoptosis +/- standard deviation. The bar graph represents an average of duplicate values of each nanoparticle concentration used to dose the cells. N=2.

TABLE 10. The percentage apoptosis observed for each zinc oxide nanoparticle concentration utilised	
ZnO Concⁿ (µg/ml)	Percentage Apoptosis (%)
1.25	28
2.5	27
5	12
10	30
25	16
50	23
100	21
TNFα/IL1β	17
MEDIA	14
-VE CONTROL	4
+VE CONTOL	100

overall percentage apoptosis is observed with the positive control, ssDNA as expected at 100%. The range of percentage apoptosis observed with the nanoparticle concentration utilised is 37% to 12% i.e. 25% **(FIGURE 18)**. The percentage apoptosis observed for each zinc oxide nanoparticle concentration utilised are presented in the **TABLE 10**.

The highest percentage apoptosis, 30% is observed with the CeO$_2$ nanoparticle concentration, 10 µg/ml. The lowest nanoparticle associated percentage apoptosis observed is associated with 5µg/ml CeO$_2$ at 12%. The lowest overall percentage apoptosis is observed with the negative control, S1 nuclease at 4%, as expected. The highest overall percentage apoptosis is observed with the positive control, ssDNA as expected at 100%. The range of percentage apoptosis observed with the nanoparticle concentration utilised is 37% to 12% i.e. 18% **(FIGURE 19)**.

Discussion

This project set out to investigate potential cytotoxic effects, the possible form of cell death induced and the likely pro inflammatory cytokine secretory phenotype in 16HBE14o bronchial epithelial cells treated with ZnO and CeO2 nanoparticles.

The major findings in light of the stated aims in section 3 are:

1. Low zinc oxide nanoparticle concentrations (2.5 µg/ml to 25 µg/ml) are pro-inflammatory, causing the secretion of increasing amount of IL-8 (32 pg/µg protein to 42 pg/µg protein) by 16HBE14o bronchial epithelial cells.

2. High zinc oxide nanoparticles concentrations (50 µg/ml to 100 µg/ml) are cytotoxic/necrotic on 16HBE14o bronchial epithelial cells, causing a reduction in percentage viability to 48% and 12% respectively.

3. Neither ZnO nor CeO$_2$ nanoparticles lead to a statistically significant secretion of IL-33 by 16HBE14o bronchial epithelial cells.

4. Low concentrations (0.01 µg/ml to 25 µg/ml) of both ZnO and CeO$_2$ nanoparticles induced significant Reactive Oxygen Species (ROS) production in 16HBE14o cells. ROS production induced by ZnO nanoparticles were significantly more than those induced by CeO$_2$ nanoparticles.

5. ZnO nanoparticles caused cell death predominantly via necrosis/cytotoxicity.

6. CeO$_2$ nanoparticles did not have any significant effect in any of the assays.

7. IL-33 is not secreted extracellularly by 16HBE14o bronchial epithelial cells treated with ZnO and CeO$_2$ nanoparticles.

8. The concentration of H$_2$O$_2$ (Hydrogen Peroxide) that stimulates ROS production in primary nasal epithelial cells (150 µM, 1 hour) does not lead to significant ROS production by 16HBE14o bronchial epithelial cells.

The finding that relatively low ZnO nanoparticle concentrations (2.5 µg/ml to 25 µg/ml) is pro-inflammatory, causing the secretion of increasing amounts of IL-8 (32 pg/µg protein to 42 pg/µg protein) by 16HBE14o bronchial epithelial cells was expected and in line with the project hypothesis. As shown in **FIGURE 14**, there is a linear and steady increase in IL-8 production (pg per µg protein) from a ZnO nanoparticle concentration of 2.5 µg/ml (32 pg/µg protein) to 25 µg/ml (42 pg/µg protein). The amount of IL-8 secreted at the ZnO NP concentration of 25 µg/ml (42 pg/µg protein) is almost identical to that secreted with the positive control and proinflammatory cytokine (TNFα/IL1β) i.e 43 pg/µg protein. Thus confirming that this is the highest concentration to induce IL-8 production in this cell line. This finding is also directly in line with a recently published paper on the inductive effect of ZnO nanoparticles on a different bronchial epithelial cell line, BEAS-2B cells. It was found that when the BEAS-2B cell line was exposed to increasing concentrations of ZnO-NPs, using similar dosing techniques as this project [39]. It significantly increased the level of IL-8 mRNA in BEAS-2B cells detected by RT-PCR and presented on an agarose gel by western blotting. Increasing ZnO-NP concentration also increased the level of IL-8 protein in supernatant medium of the BEAS-2B cell line detected using ELISA. Furthermore, Lu Y et al, 2013 showed that the inductive effect of ZnO on IL-8 production is at the level of IL-8 gene transcription [39]. This was done by using an IL-8 transcription inhibitor which resulted in a significantly reduced amount of IL-8 production when the cells were stimulated with the same concentration range of ZnO nanoparticles used without the transcription inhibitor. Previous unpublished investigative work done on A549 cells in my supervisor's laboratory (A549 cells are adenocarcinomic human alveolar basal epithelial cells.) showed a somewhat different result. Firstly the IL-8 concentration produced with the proinflammatory cytokine and positive control, TNFα/IL1β was much higher than the concentration observed in this project at 150 pg/µg protein. That observed in this project is 46 pg/µg protein. Secondly, the highest IL-8 secretion by the A549 cells(4 pg/µg protein) was much less than found in this project (44 pg/µg protein) and it was observed at the highest ZnO NP concentration used in the BEAS-2B cells (100 µg/ml) whereas in this project, the highest IL-8 secretion was found at NP concentration of 25 µg/ml. Furthermore, previous work done on primary nasal epithelial cells in the same lab show a relatively high IL-8 production at 10 µg/ml ZnO NP concentration 60 pg/µg protein, compared to IL-8 production with the positive control/proinflammatory cytokine (TNFα/IL1β) at 120 pg/µg protein.

With regards to CeO$_2$ nanoparticle, no clear trend is seen in relation to IL-8 secretion in 16HBE14o cells in this project, previous work done on A549 cells and primary nasal epithelial cells. This was a clear contrast to the in vivo result reported by Srinivas A et al., 2011 [18]. They exposed rats to increasing fume concentrations of CeO$_2$ NPs and checked for the secretion of the proinflammatory cytokines; IL1β, TNFα and IL-6. They found that the concentration of these pro inflammatory cytokines were significantly

increased in the Broncho Alveolar Lavage Fluid (BALF) and blood of the rats exposed to the CeO_2 nanoparticles.

"All substances are poisons; the dose is what determines toxicity" (Paracelsus). The finding that high ZnO nanoparticle concentrations are cytotoxic on 16HBE14o bronchial epithelial cells was also expected and in line with the project hypothesis and all literature on nanoparticle toxicity. Toxicity, measured in this project as reduced percentage viability was observed at ZnO NP concentrations of 50 μg/ml and 100 μg/ml, after a 24 hour incubation. At ZnO nanoparticle concentrations of 50 μg/ml and 100 μg/ml, after 24 hour incubation, percentage viability of the 16HBE14o cell line was greatly reduced to 49% and 12% respectively compared to 100% percentage viability achieved with media only. Kim et al, 2010 have reported alveolar epithelial cell severe injury due to zinc oxide nanoparticle exposure [36]. In their study, a much higher ZnO NP concentration, 176 μg/ml resulted in complete cytotoxicity (0.5% RT) measured as reduced trans epithelial electrical resistance in primary cultured Rat AEC Monolayers (RAECMs). Significant reduction in trans epithelial resistance was also seen at a ZnO NP concentration 44 μg/ml to 12% trans epithelial resistance (RT), very similar to the reduced percentage viability observed in this project at a ZnO NP of 100 μg/ml (i.e. 12%) Furthermore Sahu et al, 2013 have also reported toxicity induced on the human lung epithelial cell line (L-132) by zinc oxide nanoparticles [37]. They reported decreased cell viability in a concentration dependent manner between 5 μg/ml and 100 μg/ml ZnO NP concentration. Microscopic morphological examinations also revealed cell shrinkage, nuclear condensation, formation of apoptotic bodies and increased reactive oxygen parameters as ZnO NP concentration increased. Furthermore, they report increased expression of the gene, metallothionein, a biomarker associated with metal induced cytotoxicity. Previous work done in my supervisors' lab showed similar albeit reduced levels of cytotoxicity (measured as percentage cell viability) induced by ZnO NP on A549 cells. Great reductions in cytotoxicity were observed at ZnO NP concentrations of 50 μg/ml (75%) and 100 μg/ml (40%). Furthermore, in primary nasal epithelial cells, complete cytotoxicity (0% percentage cell viability) was observed at ZnO NP concentrations of 100 μg/ml.

With regards to CeO_2 NP, no significant cytotoxicity on 16HBE14o cells was observed in the dose range utilised in this project. Neither was there any in previous work done on A549 cells or primary nasal epithelial cells. This is in opposition to what was recently reported by Mittal S, 2014 on CeO_2 toxicity [41]. They dosed A549 bronchial epithelial cells with similar increasing (1 μg/ml to 100 μg/ml) CeO_2 NPs and found that after internalisation, CeO_2 caused statistically significant increase in cytotoxicity and cell death after 24 hours exposure which increased further when the cells were exposed to the same nanoparticle concentration for 48 hours. CeO_2 NP also caused morphological changes in the A549 cells. The precise mechanism of apoptotic cell death induced by CeO_2 nanoparticles on the cancerous A549 cell line was particularly effective because the cell line is cancerous. This mechanism was determined as being by DNA damage by a comet assay. It was also determined by flow cytometry analysis of the A549 cell line that CeO_2 nanoparticles leads to arrest of the cell cycle at the sub-GI phase of the cell cycle leading to apoptosis.

From these findings, it can be concluded that, the concentration of ZnO NPs is what determines whether they are pro-inflammatory or cytotoxic on 16HBE14o cells. It can also be concluded that the A549 cells are more robust, stronger and resistant to injury than 16HBE14o cells. Whilst the primary nasal epithelial cells are less robust, with potentially greater vulnerability to injury by atmospheric nanoparticles.

Putting this in the context of asthma pathogenesis; inhaling low levels of ZnO nanoparticles naturally occurring in the atmosphere over an extended period of time e.g. from birth has the potential to cause AEC injury, acute inflammation which if unresolved will lead to chronic inflammation and EMTU in susceptible individuals.

There was no significant secretion of IL-33 by 16HBE14o cells treated with a concentration range of zinc oxide and cerium dioxide nanoparticles in this project. Although Pace et al, 2014 reported IL-33 release by, 16HBE14o, cells following stimulation with cigarette smoke extract, the levels they reported were below the detection limit of the ELISA kit and should therefore be considered negative [40]. In contrast, they did find increased intracellular expression of IL-33 as confirmed by flow cytometry, western blotting and immunocytochemistry. The presence of intracellular IL-33 was also confirmed by our group using immunostaining with analysis by flow cytometry (Dr Chu Zhang - personal communication) [42,43].

These results were further corroborated by another report [19]. Using confocal microscopy, the intracellular location of IL-33 was determined in three different cell lines and using two different anti-IL33 antibodies. In contrast, report extracellular secretion of statistically significant amounts of IL-33 (using ELISA) upon applying stress and biochemical strain (1 Hz cyclic 8% biaxial stretch) to the cells [19].

In line with the hypothesis and several published literature, both ZnO and CeO_2 nanoparticles cause significant amounts of ROS production in 16HBE14o cells. Significant ROS production was observed at the low ZnO and CeO_2 nanoparticle concentrations (0.01 μg/ml to 25 μg/ml) Production was much less than at the high nanoparticle concentrations (50 μg/ml to 100 μg/ml) where cell death via necrosis (cytotoxicity) is more evident, according to the cytotoxicity results presented in **FIGURES 12 and 13**. This was in line with work done on primary nasal epithelial cells; ROS production was evident at the lower ZnO NP concentrations but not the higher cytotoxic inducing ZnO NP concentrations. Kim et al, 2010 have reported increased intracellular ROS production and a resultant loss of cell membrane integrity of alveolar epithelial cells due to zinc oxide nanoparticle exposure [36]. Sahu et al, 2013 have also reported significant increase in intracellular ROS production in L-132 human lung epithelial cells when dosed with 50 nm ZnO-NPs at concentrations between 5 and 100 μg/mL [37]. Mittal S et al, 2014 have attributed the damage to A549 bronchial epithelial cells by CeO_2 dosing to increased ROS production with a concomitant decrease in antioxidant glutathione (GSH) levels [41]. This is also in line with previous work done on primary nasal epithelial cells in my supervisor's lab. High CeO_2 concentration led to a significant amount of ROS production. In contrast, this project's reports substantial ROS production at low CeO_2 NP concentrations. The mechanism by which oxidative stress leads to ROS production and subsequent programmed cell death have led to the description of the term "Oxidative stress induced apoptosis" [37].

A novel finding of this project was that the concentration of H_2O_2 (150 μM, 1 hour) (used as the positive control) that induced significant ROS production in primary nasal epithelial cells does not cause significant ROS production in 16HBE14o cells. Therefore 16HBE14o may require a higher concentration of hydrogen peroxide or a longer incubation time to induce ROS [44,45].

The predominant method of cell death induced by high concentrations of ZnO nanoparticles (50 μg/ml to 100 μg/ml) on 16HBE14o in this project cells is necrosis/cytotoxicity. This is evident by the cytotoxicity data **FIGURE 13**. Although some insignificant levels apoptosis was evident as shown by the apoptosis assay results in **FIGURE 18**. This necrotic method of cell death and injury induced by ZnO nanoparticles is confirmed in several related studies [36,37,46]. On the other hand, with CeO_2 nanoparticles, no significant level of necrosis/cytotoxicity is evident as confirmed by the cytotoxicity data in **FIGURE 12**. Furthermore, although the highest level of apoptosis observed with CeO_2 (36%, 1.25 μg/ml) is greater than that observed with ZnO nanoparticles (28%, 10 μg/ml), the results are not statistically significant and as such cannot be relied upon. Although statistically insignificant in this project, the CeO_2 apoptosis assay results are in line with a recent publication on CeO_2 nanoparticle toxicity. Mittal S, 2014 found that the predominant form of cell death induced on A549 bronchial epithelial cells by CeO_2 nanoparticles is apoptosis [41]. The finding that CeO_2 nanoparticles cause cell death by increased

ROS leading to apoptosis was also confirmed by Park et al. 2008 [38]. They report ROS increase in cultured human lung epithelial cells (BEAS-2B) proportional to increased CeO_2 nanoparticle concentration and the subsequent activation of cytosolic caspase-3 and chromatin condensation which means that CeO_2 toxicity is via the apoptotic process.

CeO_2 did not have any noteworthy effect in any of the other assays apart from the ROS assays.

The precise mechanism and mode of ZnO NP toxicity compared to CeO_2 has been extensively studied and reported in two fairly recent and particularly relevant articles. 1) The fate of ZnO nanoparticles administered to human bronchial epithelial cells [46], and 2) Comparison of the Mechanism of Toxicity of Zinc Oxide and Cerium Oxide Nanoparticles Based on Dissolution and Oxidative Stress Properties. These studies used high resolution X-ray spectro-microscopy, high elemental sensitivity X-ray microprobe, atomic force microscopy and two different bronchial epithelial cell lines (BEAS-2B and RAW 264.7) as well as conventional lab techniques to determine the intracellular fate and form of ZnO NPs and CeO_2 NPs taken up by cells [47]. It was concluded that dissolution properties of ZnO is what leads to release of free and toxic divalent zinc ion (Zn^{2+}). ZnO toxicity is caused by free or complexed Zn^{2+} within cells. This dissolution theory of ZnO toxicity was further confirmed when the ZnO NP was dosed with 10% iron to reduce their solubility and dissolution in solvent. It was found that the Zn-Fe nanoparticles are significantly less soluble than pure ZnO nanoparticles and they were significantly less toxic than pure ZnO nanoparticles as well. Furthermore, using fluorescently labelled ZnO and a fluorescent microscope, it was found that ZnO dissolution happened in both cell culture medium and intracellularly in endosomes leading to ROS production, inflammation and cell death [46,48]. ZnO that was not dissolved entered caveolae in BEAS-2B cells but in RAW 264.7 cells they entered lysosomes. Fluorescently labelled CeO_2 nanoparticles were taken up undissolved but intact into caveolin-1 and LAMP-1 positive endosomal compartments, in BEAS-2B and RAW 264.7 cells respectively. Unlike ZnO nanoparticles, the CeO_2 nanoparticle did not split into cerium and oxygen ions. Thus did not lead to inflammation, cytotoxicity or ROS production in this study. Rather, CeO_2 curbed ROS production and prompted cellular resistance to an external source of oxidative stress [47].

Finally, there were some shortcomings in the experimental procedure which may have led to slightly inaccurate results.

1. When dosing the cells with the nanoparticles before performing the IL-33 ELISA, the culture medium was not taken out. This would have led to diluting the nanoparticles in a greater solvent than anticipated and would have led to a lower concentration of nanoparticle stimulating the cells than required. Although unlikely, this could be the reason why no significant IL-33 release was observed in the cell line.

2. As the (150 μM, 1hour) H_2O_2 did not cause significant ROS production in the 16HBE14o cell line, it would be wise to use a much higher concentration of H_2O_2 or a greater incubation time so as to cause ROS production and observe the effect of the nanoparticles on ROS production by the cell line to that of H_2O_2 on the cell line.

Conclusions

The data generated have been interesting and enlightening but should not be taken as definitive. The limited time allocated for this project meant that insufficient experimental replicates were performed. As such experiments need to be repeated before any conclusions can be made. In order to authenticate the results of this project, all the assays need to be repeated, more replicates than N=2 need to be utilised in the cytotoxicity assay. Other known atmospheric nanoparticles (copper, carbon and titanium) need to be tested in concentrations similar to their naturally occurring concentrations in the atmosphere. Furthermore, other bronchial epithelial cell lines need to be utilised and primary cells from asthmatic and non-asthmatic airways need to be utilised, dosed with these different nanoparticles and compared as well.

One major limitation of this project is the fact that the nanoparticle concentrations utilised may not be representative of real life values. Research is currently underway at the University of Birmingham to determine atmospheric levels of various nanoparticles which will vary depending on geography (country) and environment (roadside, urban or rural).

The aims of this project have been achieved to some extent but more work is required to fully answer the questions raised.

References

1. How to save our planet. Great Britain by John Murray Press. (2023).

2. Centres for Disease Control and Prevention. Climate Effects on Health. (2020)

3. Auerbach O, Stout A, Hammond EC, Garfinkel L. Changes in bronchial epithelium in relation to cigarette smoking and in relation to lung cancer. *N Engl J Med*. 265(6), 253-267 (1961).

4. Holgate ST. The sentinel role of the airway epithelium in asthma pathogenesis. *Immunol Rev*. 242(1), 205-219 (2011).

5. Chung KF, Barnes PJ. Cytokines in asthma. *Thorax*. 54(9), 825-857 (1999).

6. Finkelman FD, Hogan SP, Hershey GK, Rothenberg ME, Wills-Karp M. Importance of cytokines in murine allergic airway disease and human asthma. *J Immunol*. 184(4), 1663-1674 (2010).

7. Schuijs MJ, Willart MA, Hammad H, Lambrecht BN. Cytokine targets in airway inflammation. *Curr Opin Pharmacol*. 13(3), 351-361 (2013).

8. Shibata Y, Nakamura H, Kato S, Tomoike H. Cellular detachment and deformation induce IL-8 gene expression in human bronchial epithelial cells. *J Immunol*. 156(2), 772-777 (1996).

9. Swindle EJ, Collins JE, Davies DE. Breakdown in epithelial barrier function in patients with asthma: identification of novel therapeutic approaches. J Allergy Clin Immunol. 124(1), 23-34 (2009).

10. Puddicombe SM, Polosa R, Richter A, *et al*. Involvement of the epidermal growth factor receptor in epithelial repair in asthma. *FASEB J*. 14(10), 1362-1374 (2000).

11. Fedorov IA, Wilson SJ, Davies DE, Holgate ST. Epithelial stress and structural remodelling in childhood asthma. *Thorax*. 60(5), 389-394 (2005).

12. Holgate ST, Roberts G, Arshad HS, Howarth PH, Davies DE. The role of the airway epithelium and its interaction with environmental factors in asthma pathogenesis. Proc Am Thorac Soc. 6(8), 655-659 (2009).

13. Comer DM, Kidney JC, Ennis M, Elborn JS. Airway epithelial cell apoptosis and inflammation in COPD, smokers and nonsmokers. *Eur Respir J*. 41(5), 1058-1067 (2013).

14. Cozens A, Yezzi M, Yamaya M, *et al*. A transformed human epithelial cell line that retains tight junctions post crisis. *In Vitro Cell Dev Biol-Anim*. 28(11-12), 735-744 (1992).

15. Knight DA, Holgate ST. The airway epithelium: structural and functional properties in health and disease. *Respirology*. 8(4), 432-446 (2003).

16. Crosby LM, Waters CM. Epithelial repair mechanisms in the lung. Am J Physiol. 298(6), 715-731 (2010).

17. Holtzman MJ, Byers DE, Alexander-Brett J, Wang X. The role of airway epithelial cells and innate immune cells in chronic respiratory disease. *Nat Rev Immunol*. 14(10), 686-698 (2014).

18. Srinivas A, Rao PJ, Selvam G, Murthy PB, Reddy PN. Acute inhalation toxicity of cerium oxide nanoparticles in rats. *Toxicol Lett*. 205(2), 105-115 (2011).

19. Kakkar R, Hei H, Dobner S, Lee RT. Interleukin 33 as a mechanically responsive cytokine secreted by living cells. *J Biol Chem.* 287(9), 6941-6948 (2012).

20. Saenz SA, Taylor BC, Artis D. Welcome to the neighborhood: epithelial cell-derived cytokines license innate and adaptive immune responses at mucosal sites. *Immunol Rev*. 226(1), 172-190 (2008).

21. L Y, G K. Nanoparticles in the atmosphere. (2015).

22. Crystal RG, Randell SH, Engelhardt JF, Voynow J, Sunday ME. Airway epithelial cells: current concepts and challenges. *Proc Am Thorac Soc*. 5(7), 772-777 (2008).

23. Fu J, Dang Z, Deng Y, Lu G. Regulation of c-Myc and Bcl-2 induced apoptosis of human bronchial epithelial cells by zinc oxide nanoparticles. *J Biomed Nanotechnol*. 8(4), 669-675 (2012).

24. Lambrecht BN, Hammad H. The airway epithelium in asthma. *Nat Med*. 18(5), 684-692 (2012).

25. Heng BC, Zhao X, Xiong S, *et al*. Toxicity of zinc oxide (ZnO) nanoparticles on human bronchial epithelial cells (BEAS-2B) is accentuated by oxidative stress. *Food Chem Toxicol*. 48(6), 1762-1766 (2010).

26. Vaseem M, Umar A, Hahn Y. ZnO Nanoparticles: Growth, Properties and Application. Met oxide nanostructures their appl. 5(1), 10-20 (2010).

27. Holgate ST. Epithelium dysfunction in asthma. *J Allergy Clin Immunol*. 120(6), 1233-1244 (2007).

28. McDougall CM, Blaylock MG, Douglas JG, *et al*. Nasal epithelial cells as surrogates for bronchial epithelial cells in airway inflammation studies. *Am j respir cell mol biol*. 39(5), 560-568 (2008).

29. Miller D, Turner SW, Spiteri-Cornish D, *et al*. Culture of Airway Epithelial Cells from Neonates Sampled within 48-Hours of Birth. *PloS one*. 8(11), e78321 (2013).

30. Ehrhardt C, Kneuer C, Laue M, *et al*. 16HBE14o-human bronchial epithelial cell layers express P-glycoprotein, lung resistance-related protein, and caveolin-1. *Pharm Res*. 20(4), 545-551 (2003).

31. Forbes B, Shah A, Martin GP, Lansley AB. The human bronchial epithelial cell line 16HBE14o− as a model system of the airways for studying drug transport. *Int J Pharm*. 257(1-2), 161-167 (2003).

32. Forbes B. Human airway epithelial cell lines for in vitro drug transport and metabolism studies. *Pharm Sci Technol Today*. 3(1), 18-27 (2000).

33. Takizawa H. Impact of air pollution on allergic diseases. *Korean J Intern Med*. 26(3), 262-273 (2011).

34. Pringle EJ, Richardson HB, Miller D, *et al*. Nasal and bronchial airway epithelial cell mediator release in children. *Pediatr Pulmonol*. 47(12), 1215-1225 (2012).

35. Puchelle E, Zahm J, Tournier J, Coraux C. Airway epithelial repair, regeneration, and remodeling after injury in chronic obstructive pulmonary disease. *Proc Am Thorac Soc*. 3(8), 726-733 (2006).

36. Kim YH, Fazlollahi F, Kennedy IM, *et al*. Alveolar epithelial cell injury due to zinc oxide nanoparticle exposure. *Am j respir crit care med*. 182(11), 1398-1409 (2010).

37. Sahu D, Kannan G, Vijayaraghavan R, Anand T, Khanum F. Nanosized zinc oxide induces toxicity in human lung cells. *ISRN toxicology*. (2013).

38. Park E, Choi J, Park Y, Park K. Oxidative stress induced by cerium oxide nanoparticles in cultured BEAS-2B cells. *Toxicology*. 245(1-2), 90-100 (2008).

39. Lu Y, Xu L, Yan Z, Wu YM, Wu WD. [Inductive effect of zinc oxide nanoparticles on interleukin 8 gene expression in human bronchial epithelial cells and its regulatory mechanism]. *Chin J Ind Hyg Occup Dis*. 31(2), 117-120 (2013).

40. Pace E, Di Sano C, Sciarrino S, *et al*. Cigarette smoke alters IL-33 expression and release in airway epithelial cells. *Biochim Biophys Acta (BBA)-Mol Basis Dis*. 1842(9), 1630-1637 (2014).

41. Mittal S, Pandey AK. Cerium oxide nanoparticles induced toxicity in human lung cells: role of ROS mediated DNA damage and apoptosis. *BioMed Res Int*. 891934 (2014).

42. Scaife A, Miller D, Spiteri-Cornish D, *et al*. Inhibitory effects of Montelukast on mediator release by nasal epithelial cells from asthmatic subjects with or without allergic rhinitis. *Respir Med*. 107(12), 1859-1865 (2013).

43. Turney TW, Duriska MB, Jayaratne V, *et al*. Formation of zinc-containing nanoparticles from Zn2 ions in cell culture media: Implications for the nanotoxicology of ZnO. *Chem Res Toxicol*. 25(10), 2057-2066 (2012).

44. Wang Y, Bai C, Li K, Adler KB, Wang X. Role of airway epithelial cells in development of asthma and allergic rhinitis. *Respir Med*. 102(7), 949-955 (2008).

45. Xiao C, Puddicombe SM, Field S, *et al*. Defective epithelial barrier function in asthma. *J Allergy Clin Immunol*. 128(3), 549-556 (2011).

46. Gilbert B, Fakra SC, Xia T, *et al*. The fate of ZnO nanoparticles administered to human bronchial epithelial cells. *ACS Nano*. 6(6), 4921-4930 (2012).

47. Xia T, Kovochich M, Liong M, *et al*. Comparison of the mechanism of toxicity of zinc oxide and cerium oxide nanoparticles based on dissolution and oxidative stress properties. *Acs Nano*. 2(10), 2121-2134 (2008).

48. Zeitlin P, Lu L, Rhim J, *et al*. A cystic fibrosis bronchial epithelial cell line: immortalization by adeno-12-SV40 infection. *Am J Respir Cell Mol Biol*. 4(4), 313-319 (1991).